Supplementary Information Appendix : Hydrodynamic and entropic effects on colloidal diffusion in corrugated channels

Xiang Yang,[1] Chang Liu,[1] Yunyun Li,[2,3] Fabio Marchesoni,[2,4] Peter Hänggi,[5,6] and H. P. Zhang[1,7,*]

[1] *School of Physics and Astronomy and Institute of Natural Sciences, Shanghai Jiao Tong University, Shanghai 200240, China*

[2] *Center for Phononics and Thermal Energy Science, School of Physics Science and Engineering, Tongji University, Shanghai 200092, China*

[3] *Shanghai Key Laboratory of Special Artificial Microstructure Materials and Technology, School of Physics Science and Engineering, Tongji University, Shanghai 200092, China*

[4] *Dipartimento di Fisica, Università di Camerino, I-62032 Camerino, Italy*

[5] *Institut für Physik, Universität Augsburg, D-86135 Augsburg, Germany*

[6] *Nanosystems Initiative Munich, Schellingstrasse 4, D-80799 Müchen, Germany*

[7] *Collaborative Innovation Center of Advanced Microstructures, Nanjing 210093, China*

(Dated: August 13, 2017)

* To whom correspondence should be addressed: hepeng_zhang@sjtu.edu.cn

I. FIRST PASSAGE TIME FROM FICK-JACOBS THEORY

Let us consider the generic 1D diffusion equation,

$$\frac{\partial}{\partial t}p\left(x,t\right)=\frac{\partial}{\partial x}\left[-a(x)+\frac{\partial}{\partial x}b\left(x\right)\right]p\left(x,t\right), \tag{1}$$

for the probability density function $p\left(x,t\right)$. We denote the coordinates of two absorbing boundaries by A and B, and the unconditional First Passage Time (FPT) from any location $x_0 \in [A,B]$ to either absorbing boundary by $T(A,B|x_0)$. Then, the n-th moments of the FPT in the region $[A,B]$, $\langle T^n(A,B|x_0)\rangle$, satisfy the recursive equation [1],

$$-n\langle T^{n-1}(A,B|x_0)\rangle = a(x_0)\frac{\partial}{\partial x_0}\langle T^n(A,B|x_0)\rangle + b(x_0)\frac{\partial^2}{\partial x_0^2}\langle T^n(A,B|x_0)\rangle, \tag{2}$$

with $\langle T^0(A,B|x_0)\rangle$=1 and absorbing boundary conditions

$$\langle T^n(A,B|x_0=A)\rangle = 0, \quad \langle T^n(A,B|x_0=B)\rangle = 0. \tag{3}$$

Solving Eq. (2) with boundary conditions (3) yields [1],

$$\langle T^n(A,B|x_0)\rangle = \\ n\left[\int_{x_0}^{B}\phi(\eta)d\eta\int_{A}^{\eta}\frac{\langle T^{n-1}(A,B|\xi)\rangle}{b(\xi)\phi(\xi)}d\xi - \frac{\int_{x_0}^{B}\phi(\eta)d\eta}{\int_{A}^{B}\phi(\eta)d\eta}\int_{A}^{B}\phi(\eta)d\eta\int_{A}^{\eta}\frac{\langle T^{n-1}(A,B|\xi)\rangle}{b(\xi)\phi(\xi)}d\xi\right], \tag{4}$$

where,

$$\phi(\eta)=\exp\left(\int^{\eta}-\frac{a(\xi)}{b(\xi)}d\xi\right). \tag{5}$$

Now we specialize this general result to our case. To make contact with the Fick-Jacobs equation,

$$\frac{\partial}{\partial t}p(x,t)=\frac{\partial}{\partial x}g(x)\mathbb{D}(x)\frac{\partial}{\partial x}\frac{p(x,t)}{g(x)}, \tag{6}$$

we set $b(x)=\mathbb{D}(x)$, $a(x)=\mathbb{D}(x)g'(x)/g(x)+\mathbb{D}'(x)$ and $\phi(x)=C/[g(x)\mathbb{D}(x)]$ (C is an arbitrary constant). In our experiment, $g(x)$ and $\mathbb{D}(x)$ are even functions under mirror reflection $x\to -x$ and, therefore, $b(x)$, $\phi(x)$ are even and $a(x)$ is odd. Owing to these symmetry properties, we can simplify Eq. (4) for the FPT moments from x_0 to $\pm\triangle x$ as,

$$\langle T^n(\pm\Delta x|x_0)\rangle = n\int_{x_0}^{\Delta x}\phi(\eta)d\eta\int_{0}^{\eta}\frac{\langle T^{n-1}(\pm\Delta x|\xi)\rangle}{b(\xi)\phi(\xi)}d\xi. \tag{7}$$

where $x_0\in[0,\Delta x]$. Substituting here our expressions for $a(x)$, $b(x)$ and $\phi(x)$, for the first two moments we obtain,

$$\langle T(\pm\Delta x|x_0)\rangle = \int_{x_0}^{\Delta x}\frac{d\eta}{g(\eta)\mathbb{D}(\eta)}\int_{0}^{\eta}g(\xi)d\xi, \tag{8}$$

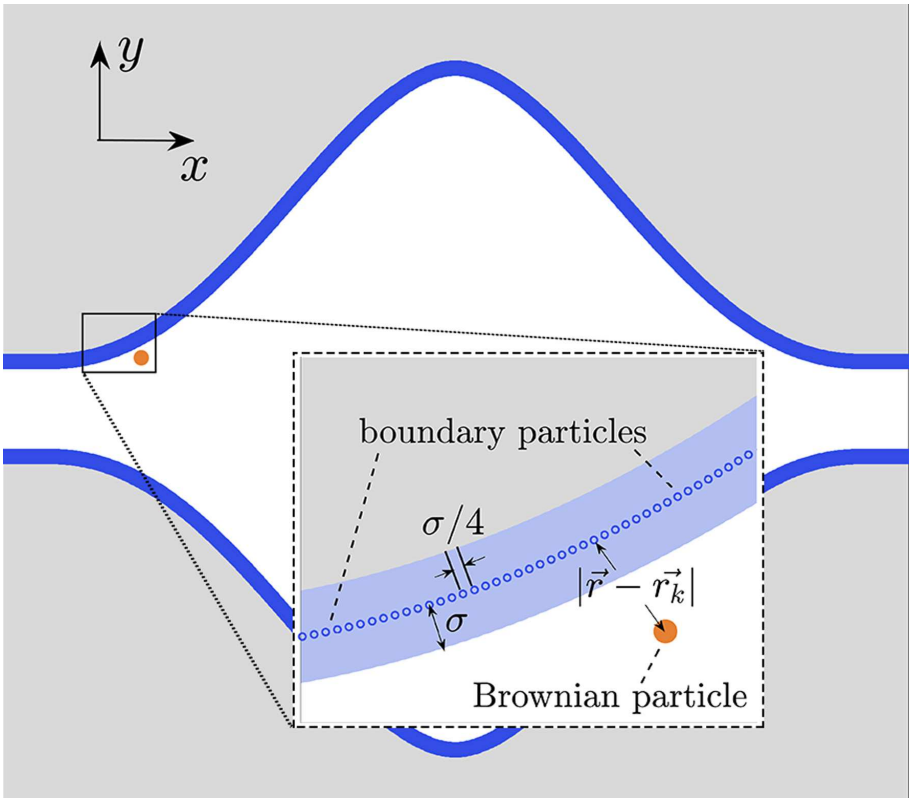

Fig. S1. Schematic diagram of the channel model used in our Brownian dynamics simulation. The fixed particles (located at $\vec{r}_k$, separated by $\sigma/4$) which mimic the walls are shown in blue and the diffusing colloidal particle (located at $\vec{r}$) in orange. The quantity σ denotes a characteristic length of the interaction potential (see text). Periodic boundary conditions are imposed at the left and right openings.

$$\langle T^2(\pm\Delta x|x_0)\rangle = 2\int_{x_0}^{\Delta x} \frac{d\eta}{g(\eta)\mathbb{D}(\eta)} \int_0^{\eta} g(\xi)\langle T(\pm\Delta x|\xi)\rangle d\xi, \tag{9}$$

and, finally, setting $x_0 = 0$, the corresponding expressions reported in the main text.

II. BROWNIAN DYNAMICS SIMULATION

Motion of the colloidal particle is governed by an overdamped Langevin equation:

$$\frac{d\vec{r}}{dt} = -\frac{D_{hyd}(x)}{k_B T}\sum_k \nabla U(|\vec{r} - \vec{r}_k|) + \vec{\xi}(t), \tag{10}$$

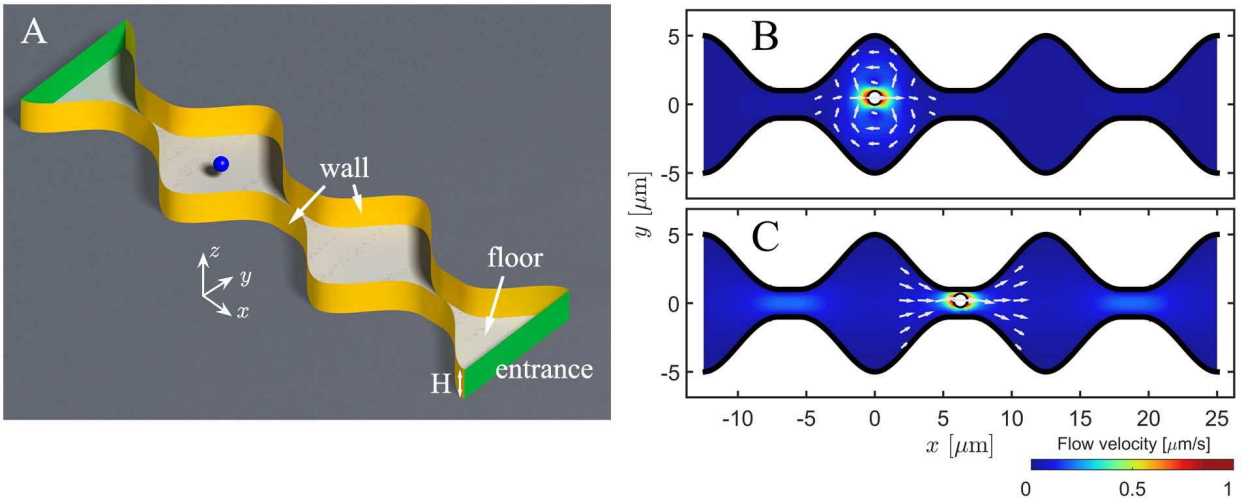

Fig. S2. Finite-element simulation for a confined sphere: Schematic diagram of the model (A); flow field in the channel as the particle moves in the open region, (B) and through a bottleneck, (C), of the channel. Magnitude and direction of the flow around the particle are represented on a color scale and by white arrows, respectively. Particle's coordinates are $(x, y) = (0, 0.47)\mu$m in (b) and $(x, y) = (6.2, 0.2)\mu$m in (c). The channel geometry is as in Fig. 1 B.

where $\vec{\xi}(t)$ is a multiplicative Gaussian white noise with $\langle \xi_i(t) \rangle = 0$ and $\langle \xi_i(t+\tau)\xi_j(t) \rangle = 2D_{hyd}(x)\delta(\tau)\delta_{ij}$ $(i, j = x, y)$. As shown in Fig. S1, the channel boundary is represented by a string of fixed particles, which interact with the colloidal particle via a short-range repulsive force. The corresponding pair potential, $U(|\vec{r} - \vec{r_k}|)$, depends on the relative distance between the colloidal $(\vec{r})$ and k-th wall $(\vec{r_k})$ particle, that is

$$U(r) = \begin{cases} U_{LJ}(r) - U_{LJ}(1.12\sigma), \ r \leq 1.12\sigma \\ 0, \ r > 1.12\sigma \end{cases} \tag{11}$$

$$U_{LJ}(r) = 4\varepsilon[(\frac{\sigma}{r})^{12} - (\frac{\sigma}{r})^{6}], \tag{12}$$

where ε and σ are, respectively, the strength and characteristic length of the Lennard-Jones(LJ) potential $U_{LJ}(r)$.

We had recourse to Euler's method to discretize the Langevin equation with a time step dt. Let us consider the motion in the x direction and denote the x component of the force $-\sum_k \nabla U(|x - x_k|)$ by $F(x)$. Integrating the Langevin equation, we have :

$$x(t+dt) = x(t) + \int_t^{t+dt} \frac{D_{hyd}(x(s))}{k_B T} F(x(s))ds + \int_t^{t+dt} \sqrt{2D_{hyd}(x\,(s))}\;\eta(s)ds, \qquad (13)$$

where $\eta(s)$ is a Gaussian white noise with zero mean and unit variance. For thermodynamic consistency, we used the transport (also known as kinetic or isothermal) convention [2–4] (see also Sections 2.4 and 6.2 in [5]) to calculate the stochastic integral [4, 6]: $\int_t^{t+dt} \sqrt{2D_{hyd}(x(s))}\,\eta(s)ds = \sqrt{2D_{hyd}(x(t+dt))dt}\,\eta_0(t)$, where $\eta_0(t)$ is a Gaussian random number with unit variance. With the transport convention, the right-hand side of Eq. (13) contains the post-point value, i.e., $x(t+dt)$, and we used a predictor-corrector scheme [7] to compute this quantity:

$$x^*(t+dt) = x(t) + \frac{D_{hyd}(x(t))}{k_B T} F(x(t))dt + \sqrt{2D_{hyd}(x(t))dt}\;\eta_0(t). \qquad (14)$$

Substituting Eq. (14) into the right-hand side of Eq. (13), we have

$$x(t+dt) = x(t) + \frac{D_{hyd}(x^*(t+dt))}{k_B T} F(x^*(t+dt))dt + \sqrt{2D_{hyd}(x^*(t+dt))dt}\;\eta_0(t). \qquad (15)$$

The discretized equation in the y direction has a similar form as Eq. (15). Our numerical scheme produces uniformly distributed Brownian particles under the condition of a spatially varying diffusivity, which validates the scheme.

We used a time step $dt = 0.2$ ms, while for $D_{hyd}(x)$ we made use of the experimentally measured diffusivity function. In addition, we set $\sigma = 0.1\,\mu$m and $\varepsilon = 2k_BT$ in the potential $U_{LJ}(r)$, and located the wall particle $\vec{r}_k$, so that the space accessible to the diffusing colloidal particle was same as that in experiments. If we nondimensionalize length, time, and energy, respectively, by L, $\frac{L^2}{D_0}$ and k_BT, the dimensionless parameters are $\sigma = 8\times10^{-3}$, $dt = 4\times10^{-7}$, and $\varepsilon = 2$. Particle trajectories from simulations were analyzed in the same way as its experimental counterpart to determine the relevant FPT's.

III. FINITE-ELEMENT CALCULATION

We employed a finite-element package (COMSOL Multiphysics v5.1) to compute the drag force on a moving sphere in a confined channel. The Stokes equations were solved in a domain shown in Fig. S2 A. No-slip boundary conditions are imposed on the side walls,

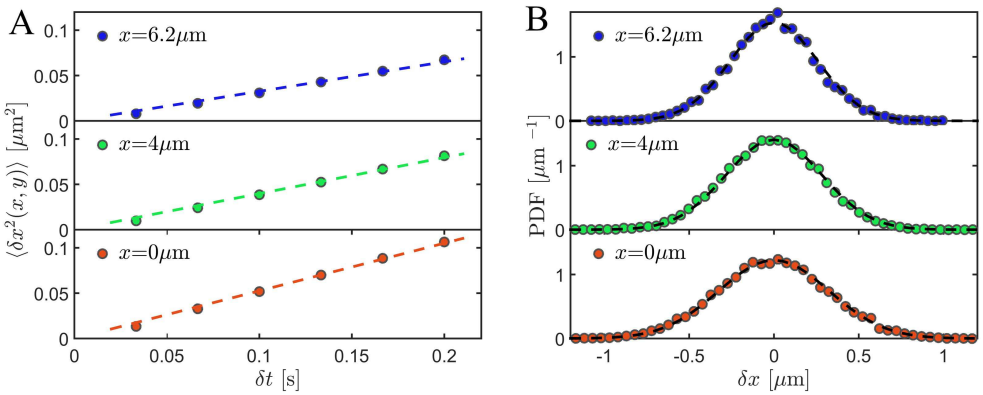

Fig. S3. (A) Mean-squared displacement $\langle \delta x^2(x,y) \rangle$ vs. δt at different x along the center line of the channel ($y = 0$). Linear fits are used to extract $D_x(x, 0)$; (B) Probability distributions of δx at time $\delta t = 0.2$ s fitted by Gaussian functions (solid curves) of corresponding variance $\langle \delta x^2(x,y) \rangle$. The channel parameters are the same as in Fig. 2 B.

floor and ceiling (not shown), while open boundary conditions are adopted for the channel openings. The geometry of the side wall is set to reproduce the inner channel boundary measured in the experiments [see insert of Fig. 1 A]; the distance between the floor and ceiling is 2.5μm. The sphere was made to move with a constant x-velocity, $v_x = 1\mu$m/s, at different locations in a horizontal plane, a distance 1.25μm over the floor. We used about half million elements in the simulation to ensure convergence. The same numerical method was followed to solve the problem of a sphere moving in a long cylinder; here, the computed drag force on the sphere deviates by less than 5% from the analytical predictions.

At any given point in the plane $z = 1.25\mu$m, we first computed the drag force f_x, then the hydrodynamic friction coefficient in the x direction, $\gamma(x, y) = f_x/v_x$, and, finally, through the fluctuation-dissipation theorem, the diffusion coefficient, $D(x, y) = k_B T/\gamma(x, y)$, which assumes the off-diagonal element of the hydrodynamic friction tensor is small. This assumption holds throughout the computational domain except in regions very close to sloping boundaries and leads to a small error, less than 2%, in computed D_{hyd} plotted in Fig. 4 C.

IV. LOCAL DIFFUSIVITY MEASUREMENTS

Hydrodynamic interactions with boundaries cause the diffusion coefficient to change spatially inside the channel. We measured the local diffusion coefficient through the mean-

squared displacement law, $\langle \delta x^2(x,y) \rangle = 2D(x,y)\delta t$. As shown in the example of Fig. S3 A, for $\delta t < 0.2$ s, the mean-squared displacements at three locations increase linearly with time, which allow us to determine the local value of $D(x,y)$. In Fig. S2 B, we plotted the corresponding probability distributions of δx at time $\delta t = 0.2$ s. All distributions are fitted by a Gaussian function with the relevant variance $\langle \delta x^2 \rangle$. The choice $\delta t = 0.2$ s is optimal for our purpose: it is long enough to yield $D(x,y)$ measurements with a high signal-to-noise ratio, but also so short that the particle displacement is limited and spatial heterogeneity due to channel's corrugation negligible.

---

[1] Goel, N. S. & Richter-Dyn, N. *Stochastic Models in Biology* (Academic Press Inc., New York, 1974).

[2] Farago, O. & Gronbech-Jensen, N. Langevin dynamics in inhomogeneous media: Re- examining the Itô-Stratonovich dilemma. *Phys. Rev. E* **89**, 013301 (2014).

[3] Sokolov, I. M. Itô, Stratonovich, Hänggi and all the rest: The Thermodynamics of interpretation. *Chem. Phys.* **375**, 359–363 (2010).

[4] Hänggi, P. Stochastic processes. I. Asymptotic behaviour and symmetries. *Helv. Phys. Acta* **51**, 183–201 (1978).

[5] Hänggi, P. & Thomas, H. Stochastic processes: time evolution, symmetries and linear response. *Phys. Rep.* **88**, 207–319 (1982).

[6] van Kampen, N. G. Itô versus Stratonovich. *J. Stat. Phys.* **24**, 175–187 (1981).

[7] Bruti-Liberati, N. & Platen, E. Strong predictor–corrector Euler methods for stochastic differential equations. *Stochastics and Dynamics* **8**, 561–581 (2008).